第 50 卷 第 24 期/2023 年 12 月/中国激光 研究论文

中国激光

RB-SiC 表面飞秒激光烧蚀与抛光工艺研究

陈欢[1,2]，魏朝阳[1,2*]，曹珍[1,2**]，彭小聪[1,2]，邵建达[1,2]
[1]中国科学院上海光学精密机械研究所精密光学制造与检测中心，上海 201800；
[2]中国科学院大学材料与光电研究中心，北京 100049

摘要 首先基于一维双温模型阐明了飞秒激光与 RB-SiC 表面的相互作用过程，并在此基础上，开展了 RB-SiC 表面飞秒激光烧蚀规律与抛光工艺研究。结果表明，通过改变脉冲能量、扫描速度、扫描间距等参数，可实现对烧蚀深度和烧蚀表面质量的有效调控。但是通过飞秒激光抛光难以在 RB-SiC 切割表面上获得较高的表面质量，而对于 RB-SiC 预抛光表面，通过工艺参数调控，可将其表面粗糙度从 36.9 nm 抛光至 11.56 nm，验证了飞秒激光抛光 RB-SiC 的可行性。

关键词 激光技术；粗糙度；反应烧结碳化硅；飞秒激光抛光；双温模型
中图分类号 TN249 **文献标志码** A **DOI**：10.3788/CJL230657

1 引 言

碳化硅（SiC）陶瓷具有高热导率、低热畸变[1]等优点，且热稳定性高于玻璃[2-3]、铝[4-5]、铍[6-7]等材料，因此在空间反射镜研究中得到了广泛的应用，是目前制作大口径镜片的理想材料[1]。而反应烧结碳化硅（RB-SiC）作为 SiC 陶瓷的一种，易于制成形状复杂的大尺寸镜胚，例如轻量化蜂窝结构等[8]，有望成为大尺寸光学望远镜的优选材料[9]，在超高分辨力天文观测、深空探测以及空间态势感知等领域中有着广阔的应用前景。然而，其高硬度及复相结构（含有质量分数约为 30% 的硅[10]）给 RB-SiC 反射镜的制造带来了巨大的挑战。尽管现有抛光技术可以得到质量很高的 RB-SiC 表面，能够满足 RB-SiC 反射镜的粗糙度和面形精度要求[11-12]，但其抛光效率很低，制造周期长，成本高[8,13]。磨粒抛光技术是 RB-SiC 表面处理中普遍采用的一种抛光技术，多选用硬度比 RB-SiC 高的金刚石磨粒作为磨料，利用犁削和滑擦作用实现表面材料去除[14]，国内外对 RB-SiC 磨料抛光技术也进行了大量的研究[12-13,15-17]，以提高其表面质量。康念辉等[18]采用磨粒抛光技术将直径为 60 mm 的 RB-SiC 表面抛光至粗糙度为 1.525 nm，但 RB-SiC 的高硬度导致的抛光效率问题也较为突出，需要 4 h 将表面粗糙度从 41.306 nm 降至 18.753 nm，而将表面粗糙度从 18.753 nm 降至 1.525 nm 花费了 10 h。为了进一步提高 RB-SiC 表面的抛光质量和抛光效率，研究人员提出了外场辅助作用下的复合加工方法[19-23]。通过表面氧化和预裂纹降低碳化硅的抛光难度，表面氧化后的二氧化硅相对于碳化硅更容易被去除，而预裂纹则有利于提高其抛光效率，目前关于此方法的研究主要集中在单晶 SiC 上。Yin 等[23]在 SiC 单晶上进行了阳极氧化和机械抛光的复合工艺研究，通过电化学方法进行阳极化，可以在 SiC 的表面上形成一层易于清除的氧化硅，然后用机械方法进行抛光，得到了粗糙度为 15.1 nm 的 SiC 表面。然而，RB-SiC 存在的两相结构对于外场辅助技术是一个巨大的挑战。两相材料的去除、氧化特性差异会造成表面氧化及预裂纹处理过程中的均匀性问题，对氧化与裂纹过程的可控性带来了巨大的挑战，使得辅助抛光工艺变得更加复杂。

激光具有非接触、高可控、高质量、高效率等优点[24-25]，已成为一种重要的抛光工具[26]，尤其是脉冲激光精密抛光[27-28]，已在高硬度材料表面上得到了一定的应用[29]。例如，研究人员开展了激光扫描速度和平均功率对钕铁硼表面加工形貌的影响研究[30]。而飞秒激光作为一种极具应用前景的高精密加工工具，有望解决 RB-SiC 的两相结构和高硬度带来的传统的抛光工艺效率较低的问题。研究人员对飞秒激光抛光 SiC 陶瓷进行了初步的研究，并提出了利用飞秒激光对 SiC 陶瓷进行水下抛光的新工艺[31-32]。首先，研究人员研究了烧蚀深度和表面粗糙度随飞秒激光频率、脉冲能量的变化规律[31]，发现烧蚀深度随着激光频率及脉冲能量的增大呈现先增大后降低的变化规律，而随着脉冲能量的增加，表面粗糙度先减小后增加。通过脉冲能量和激光频率的参数优化，得到了平均表面粗糙度为 0.72 μm 的表面。然后，研究人员通过试验分析

收稿日期：2023-03-28；**修回日期**：2023-06-20；**录用日期**：2023-07-12；**网络首发日期**：2023-08-07
基金项目：国家自然科学基金天文联合基金重点（U1831211）、上海市青年科技英才扬帆计划（20YF1454800）
通信作者：*siomwei@siom.ac.cn；**caozhen@siom.ac.cn

了扫描间距对表面粗糙度的影响[32]，发现在 15 μm 的扫描间距下可以得到平滑的表面。

但飞秒激光在RB-SiC中的应用研究却鲜有报道，其与RB-SiC之间的作用过程和烧蚀规律还不清楚。因此，需要对飞秒激光与RB-SiC的作用过程进行进一步的理论分析和试验研究。本文以双温模型为基础，通过对RB-SiC中两相的电子温度、晶格温度与电子-声子耦合热传导过程的分析，阐明了飞秒激光与RB-SiC的相互作用过程。其次，研究了RB-SiC在飞秒激光作用下的烧蚀规律。理解和掌握飞秒激光扫描过程中各工艺参数对RB-SiC烧蚀的影响规律，可为飞秒激光表面精密抛光提供一定的技术指导。在此基础上，初步探索了RB-SiC表面飞秒激光抛光的工艺参数，为其作为抛光工具在RB-SiC表面抛光中的应用提供了理论基础和试验依据。

2 试验装置与理论模型

2.1 试验装置

试验采用的飞秒激光直写加工系统主要由飞秒激光器、气浮移动平台、光学系统、机械系统和控制系统等部分组成，其示意图如图1(a)所示，扫描路径示意图如图1(b)所示，其中 Δy 为扫描间距，v 为扫描速度，Φ 为光斑直径。光源使用的飞秒激光器具有 1030 nm 的中心波长，290 fs 的脉冲宽度，15 W 的最大平均功率，200 μJ 的最大脉冲能量和 1 kHz～1 MHz 的重复频率。通过偏振分束器将激光光束分为两个部分，其中 S 偏振光束用于实际的加工。此外，光束聚焦模块装备有一个数值孔径为 0.14 的 5× 物镜，可将激光光束直径聚焦至 12 μm($1/e^2$)，其光斑能量近似呈高斯分布。

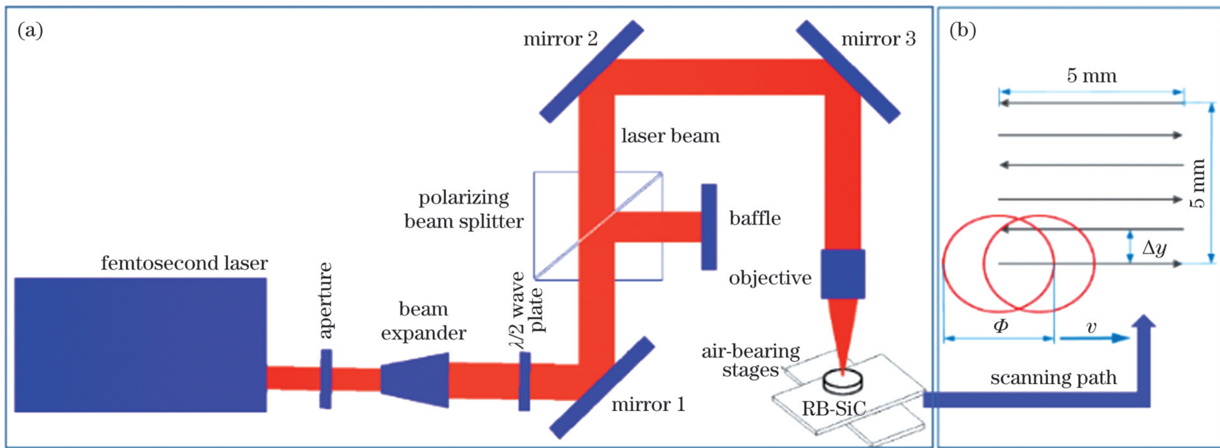

图1　试验装置和扫描路径。(a)飞秒激光直写加工系统示意图；(b)扫描路径示意图

Fig. 1　Test device and scanning path. (a) Schematic of femtosecond laser direct writing processing system; (b) scanning path

试验所用的材料是 RB-SiC，切割后尺寸为 Φ30 mm×4 mm。其中，对部分RB-SiC样品表面进行约 32 h的化学机械抛光，以进行飞秒激光抛光工艺研究；而其余样品则保持了原有的切割形态，用于表面烧蚀试验研究。光滑表面的粗糙度和形貌由4D轮廓仪进行测量，测试区域尺寸为 0.2 mm×0.2 mm，粗糙表面的粗糙度和烧蚀深度由轮廓仪进行测量。

2.2 理论模型

当飞秒激光与物质相互作用时，光子主要被电子吸收，由于电子变为离子的时间尺度是皮秒级(10^{-12}～10^{-10} s)，故晶格运动在飞秒脉冲持续时间内可以忽略不计，只考虑光子-电子之间的相互作用[33]。本文基于一维双温模型，定性地分析了飞秒激光与RB-SiC相互作用的过程。通过对飞秒激光作用下电子及晶格温度变化的计算，分析了不同脉冲能量作用下晶格温度的演化过程，进而判断激光脉冲能量与RB-SiC烧蚀程度之间的关系。一维双温模型的两个非线性微分方程[34]可表示为

$$C_e \cdot \frac{\partial T_e}{\partial t} = K_e \cdot \frac{\partial^2 T_e}{\partial x^2} - g \cdot (T_e - T_l) + S(x,t), \tag{1}$$

$$C_l \cdot \frac{\partial T_l}{\partial t} = K_l \cdot \frac{\partial^2 T_l}{\partial x^2} + g \cdot (T_e - T_l), \tag{2}$$

式中：C_e 和 C_l 分别为电子和晶格的热容；T_e 和 T_l 分别为电子和晶格的温度；K_e 和 K_l 分别为电子和晶格的热导率；g 为电子-声子耦合系数；$S(x,t)$ 为高斯脉冲激光热源在 x 处的能量，t 为时间。$S(x,t)$ 的表达式[35]为

$$S(x,t) = \sqrt{\frac{4 \cdot \ln 2}{\pi}} \cdot \frac{1-R}{L_p \cdot t_p} \cdot \frac{E}{\pi \cdot r_0^2} \cdot \exp\left[-\frac{x}{L_p} - 4\left(\frac{t - 2 \cdot t_p}{t_p}\right)^2 \ln 2\right], \tag{3}$$

式中：R 为反射率；L_p 为趋肤深度；E 为飞秒激光单脉冲能量；r_0 为飞秒激光聚焦光斑直径($1/e^2$)；t_p 为飞秒激光脉宽。

采用有限元法对一维双温模型进行求解，假定晶格和电子的初始温度为 300 K，边界条件为

$$C_e \cdot \frac{\partial T_e}{\partial t}\Big|_x = C_l \cdot \frac{\partial T_l}{\partial t}\Big|_x = 0。 \tag{4}$$

设定 R、C_e、C_l、K_e 和 K_l 均为常数，假设它们不会随着温度的变化或者等离子体的形成而改变，因此简化了模型的计算。该模型仅用于定性分析飞秒激光作用过程中的温度变化，进而描述飞秒激光作用过程。由于 RB-SiC 具有复相特性，我们分别计算分析了 SiC 和 Si 的烧蚀过程。模型中使用的 SiC 和 Si 的物理参数值如表 1 所示，模型采用的脉冲宽度为 290 fs，光斑直径为 12 μm。通过改变脉冲能量，分析了飞秒激光烧蚀与脉冲能量之间的关系。

表 1 模型中使用的 SiC 和 Si 的物理参数

Table 1 Physical parameters of SiC and Si used in model

Physical parameter	Symbol	Unit	Value	
			SiC[36-37]	Si[38-39]
Electron-phonon coupling strength	g	W /(m³·K)	1.12×10^{17}	2.07×10^{17}
Heat capacity of electron	C_e	J /(m³·K)	78.3	103.575
Thermal conductivity of electron	K_e	J /(m·K·s)	27.3	158.3
Heat capacity of lattice	C_l	J /(m³·K)	1.659×10^{5}	2.08×10^{5}
Thermal conductivity of lattice	K_l	J /(m·K·s)	1.48	3.24
Reflectance	R		0.8	0.327
Depth of ballistic transportation	L_p	m	1.37×10^{-9}	9.8×10^{-6}

3 结果与讨论

3.1 基于理论模型的作用过程分析

将飞秒激光脉冲能量设定为 0.25 μJ，即能量密度为 0.221 J/cm^2，RB-SiC 中 SiC 相和 Si 相的电子与晶格的温度随时间的变化如图 2 所示。在飞秒激光单脉冲作用下，电子温度迅速升高，并迅速达到峰值。在此期间，电子-声子耦合作用使得晶格温度不断升高，电子温度下降，直到电子温度和晶格温度达到平衡。另外，从图 2 可以看出，当电子与晶格温度达到平衡状态时，SiC 的晶格温度比 Si 的晶格温度要低得多。比较 RB-SiC 中 SiC 和 Si 的电子温度、晶格温度、电子-声子耦合和热传导过程，有助于了解飞秒激光与 RB-SiC 的作用过程。同时，通过改变飞秒激光单脉冲能量，预测了 SiC 相和 Si 相的晶格温度随脉冲能量的变化规律，如图 3 所示。当脉冲能量增大时，达到平衡时的晶体温度逐渐升高，表明 RB-SiC 表面的烧蚀程度随脉冲能量的增大而增大。

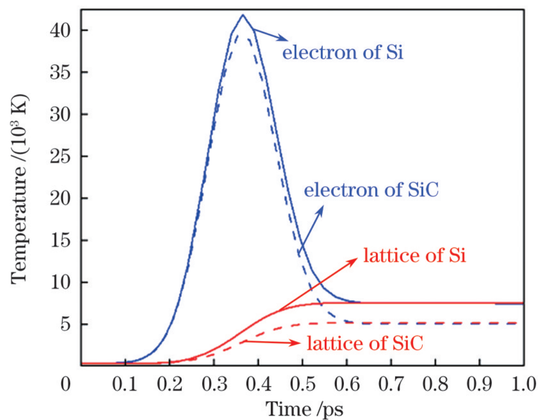

图 2 SiC 和 Si 的电子与晶格的温度随时间的变化

Fig. 2 Temperature versus time for electrons and lattices of SiC and Si

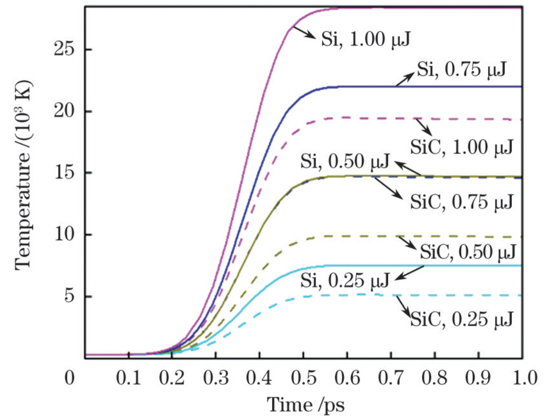

图 3 不同脉冲能量值下 SiC 和 Si 的晶格温度

Fig. 3 Temperatures of lattices of SiC and Si under different pulse energy values

此外，通过改变飞秒激光脉冲能量，研究了 RB-SiC 的飞秒激光单脉冲烧蚀，将脉冲能量设为 1.39～3.49 μJ，烧蚀形貌如图 4(a)所示。可以看出，随着脉冲能量的增加，烧蚀更加剧烈，3.49 μJ 脉冲能量下产生的烧蚀凹痕较为明显，而 1.39 μJ 脉冲能量下的烧蚀程度相比 3.49 μJ 则较弱。另外，烧蚀凹坑的直径与脉冲能量的关系如图 4(b)所示。其中，每个能量下各烧蚀三次，用显微镜测量它们的烧蚀直径，以平均值作为烧蚀直径，标准差作为测量误差。可以看出，脉冲能量越大，烧蚀凹坑直径越大，1.39 μJ 脉冲能量下能得到直径约为 12.7 μm 的烧蚀凹坑，而 3.49 μJ 脉冲能量下产生的烧蚀凹坑直径约为 16 μm。

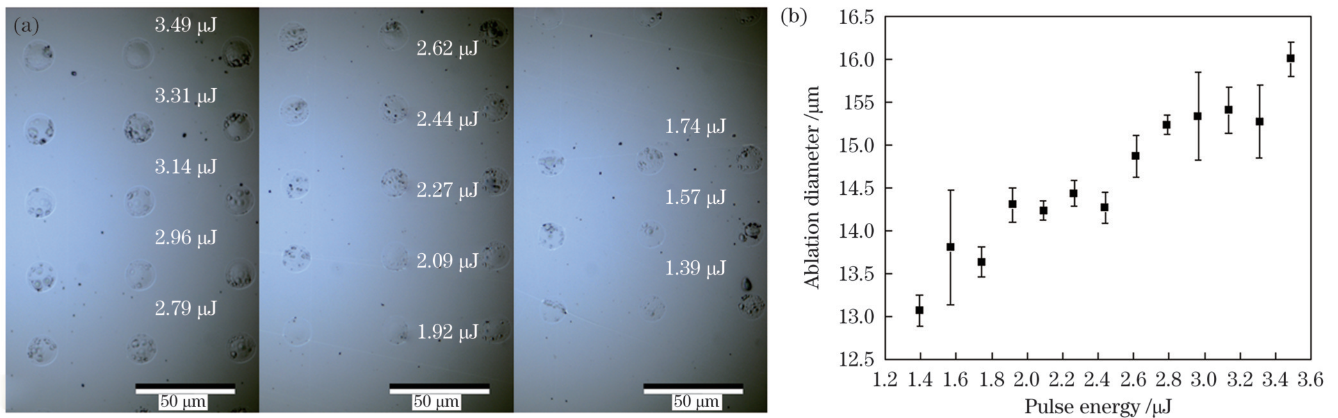

图4　不同脉冲能量值下RB-SiC的飞秒激光单脉冲烧蚀结果。(a)单脉冲烧蚀形貌；(b)烧蚀直径与脉冲能量的关系

Fig. 4　Femtosecond laser single pulse ablation results of RB-SiC under different pulse energy values. (a) Single pulse ablation morphologies; (b) relationship between ablation diameter and pulse energy

飞秒激光单脉冲烧蚀试验表明，烧蚀凹坑直径随着脉冲能量的增加而增大。说明随着脉冲能量的增加，烧蚀程度加剧，这与双温模型得到的烧蚀规律是一致的。另外，飞秒激光的单脉冲烧蚀区面积增大，其原因是当脉冲能量增加时，烧蚀区域的能量增加，烧蚀凹坑增加。

3.2　区域烧蚀试验

通过区域烧蚀探究了4个主要激光参数（激光能量E、激光频率f、扫描速度v和扫描间距Δy）对烧蚀深度、表面粗糙度和表面形貌的影响。飞秒激光烧蚀区域尺寸是5 mm×5 mm，其扫描轨迹如图1(b)所示。

首先，通过改变脉冲能量，分析其对区域烧蚀的影响规律。将飞秒激光区域扫描参数设定为：扫描速度v是5 mm/s，激光频率是100 kHz，扫描间距Δy是0.015 mm，脉冲能量是0.51～4.65 μJ，区域烧蚀结果如图5所示。由图5(a)可见，脉冲能量对烧蚀区域的表面粗糙度的影响很大，烧蚀区域的表面粗糙度随脉冲能量的增大而增加，RB-SiC初始表面的表面粗糙度为0.13 μm，经过脉冲能量为0.51 μJ的飞秒激光扫描后，表面粗糙度达到0.61 μm；当脉冲能量达到4.65 μJ时，它的表面粗糙度可达2.12 μm，约是初始表面粗糙度的20倍。另外，不同脉冲能量下的烧蚀深度如图5(b)所示，随着脉冲能量的增加，烧蚀深度也不断增加，并且增长速度较大，0.51 μJ脉冲能量下烧蚀区域的烧蚀深度约为2.7 μm，而4.65 μJ脉冲能量下的烧蚀深度为7.8 μm，是0.51 μJ脉冲能量下产生的烧蚀深度的2倍多。

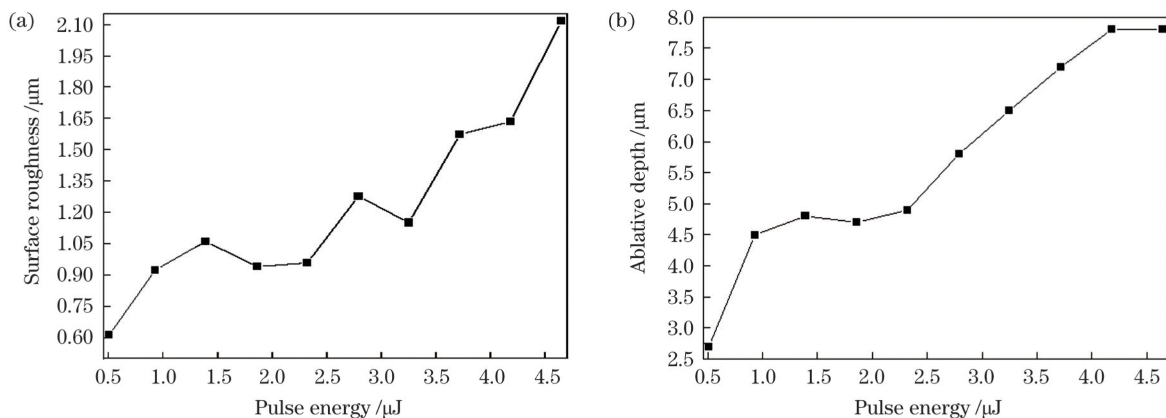

图5　不同脉冲能量下区域烧蚀试验结果。(a)烧蚀区域的表面粗糙度；(b)烧蚀区域的烧蚀深度

Fig. 5　Regional ablation test results under different pulse energy values. (a) Surface roughness of ablation area; (b) ablative depth of ablative area

其次，我们通过脉冲频率和扫描速度的组合试验，研究了扫描速度和脉冲频率对RB-SiC表面区域烧蚀的影响，脉冲能量设定为2.32 μJ，扫描间距设定为0.015 mm，脉冲频率f和扫描速度v的设定如表2所示。试验结果如图6所示，当扫描速度和脉冲频率都设定为较高值时，烧蚀区域的表面粗糙度比较大[图6(a)]，而当扫描速度为4 mm/s、脉冲频率为1000 kHz时烧蚀区域具有最大表面粗糙度5.6 μm。另外，在低脉冲频率(10～50 kHz)条件下，扫描速度对表面粗糙度的影响不大，所有烧蚀区域的表面粗糙度都在0.4 μm左右。表面烧蚀深度如图6(b)所示，表现出的规律与表面粗糙度相

表2 脉冲频率和扫描速度的参数设置

Table 2 Parameter settings of pulse frequency and scanning speed

Pulse frequency /kHz	Scanning speed /(mm/s)
1000.00	0.8,1.6,2.4,3.2,4.0,4.8,5.6,6.4,7.2,8.0
500.00	0.8,1.6,2.4,3.2,4.0,4.8,5.6,6.4,7.2,8.0
333.33	0.8,1.6,2.4,3.2,4.0,4.8,5.6,6.4,7.2,8.0
250.00	0.8,1.6,2.4,3.2,4.0,4.8,5.6,6.4,7.2,8.0
200.00	0.8,1.6,2.4,3.2,4.0,4.8,5.6,6.4,7.2,8.0
166.67	0.8,1.6,2.4,3.2,4.0,4.8,5.6,6.4,7.2,8.0
125.00	0.8,1.6,2.4,3.2,4.0,4.8,5.6,6.4,7.2,8.0
100.00	0.8,1.6,2.4,3.2,4.0,4.8,5.6,6.4,7.2,8.0
50.00	0.8,1.6,2.4,3.2,4.0,4.8,5.6,6.4,7.2,8.0
10.00	0.8,1.6,2.4,3.2,4.0,4.8,5.6,6.4,7.2,8.0

似。通过对表面粗糙度和烧蚀深度进行对比分析，可以看出，烧蚀深度越浅，表面粗糙度越小，也就是说，为了获得更低的表面粗糙度，必须有更小的去除量。

由于扫描间距是实现烧蚀表面平坦化的关键因素，设置脉冲频率为 100 kHz，脉冲能量为 0.51 μJ，扫描速度为 2 mm/s，研究了不同扫描间距 Δy 对 RB-SiC 烧蚀区域表面粗糙度和烧蚀形貌的影响。试验结果如图 7 所示，随着扫描间距 Δy 的增加，表面粗糙度持续增加。当扫描间距为 0.02 mm 时，表面粗糙度为 1.82 μm，而当扫描间距为 0.005 mm 时，烧蚀区域的表面粗糙度为 0.304 μm，后者约是前者的 16%。

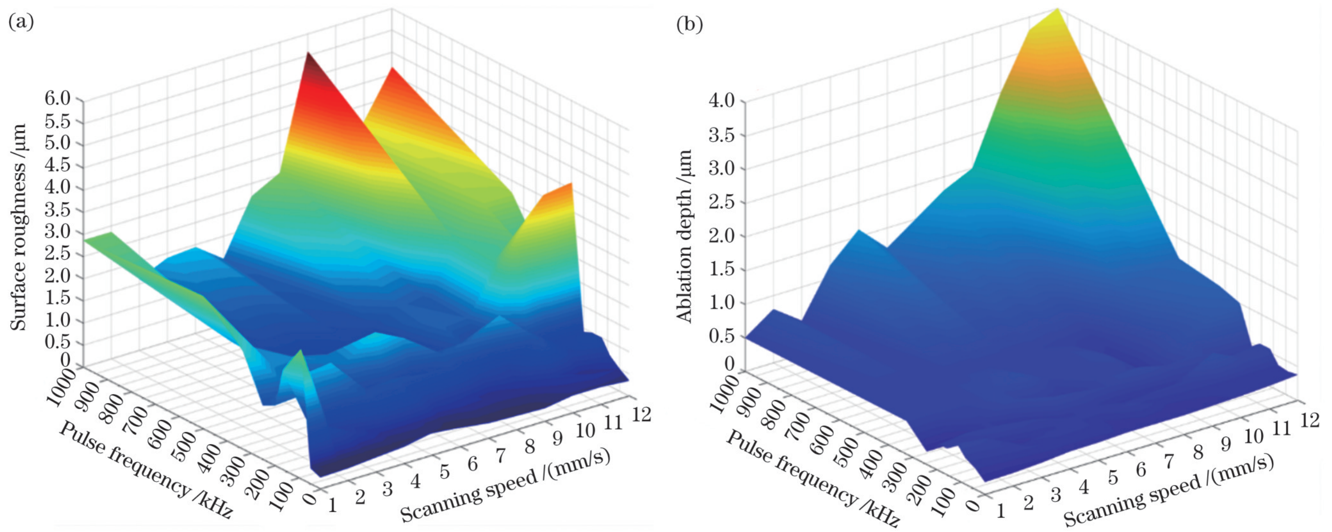

图6 扫描速度和脉冲频率对 RB-SiC 表面区域烧蚀的影响。(a)表面粗糙度；(b)烧蚀深度

Fig. 6 Effects of scanning speed and pulse frequency on ablation of RB-SiC surface area. (a) Surface roughness; (b) ablation depth

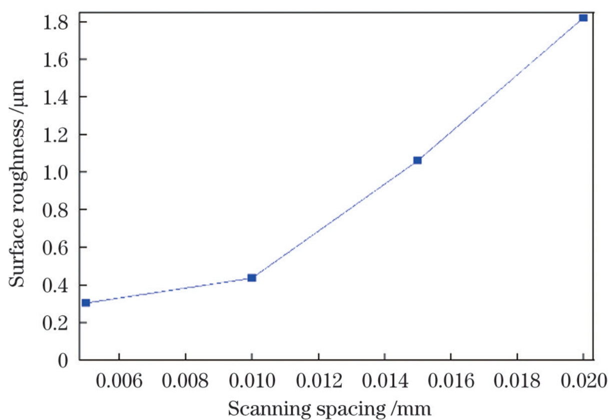

图7 不同扫描间距下烧蚀区域的表面粗糙度

Fig. 7 Surface roughness of ablation area at different scanning spacing

区域烧蚀研究结果表明，激光能量、激光频率、扫描速度、扫描间距等因素对烧蚀深度、表面粗糙度及表面形貌均有不同程度的影响。随着脉冲能量的增加，烧蚀表面的表面粗糙度和烧蚀深度不断增加，并且烧蚀深度越深，表面粗糙度就会变得越大。扫描速率、激光频率对光斑的搭接率有直接的影响，较大的光斑搭接率会导致较深的刻蚀深度和较大的烧蚀表面粗糙度，但较小的扫描间距有利于获得平坦的烧蚀表面。此外，烧蚀区域的表面粗糙度结果表明，通过飞秒激光抛光难以在 RB-SiC 切割表面上获得较高的表面质量。

3.3 抛光工艺研究

在 RB-SiC 表面烧蚀研究的基础上，用 CeO_2 抛光液对 RB-SiC 切割表面进行约 32 h 的抛光预处理，并利用该预抛光表面进行飞秒激光精密抛光工艺研究。将激光能量设置为 0.09 μJ，扫描速率设置为 9.6 mm/s，激光重复频率设置为 40 kHz，研究当扫描间隔为 0.0018、0.0012、0.0006、0.0002 mm 时 RB-SiC 表面粗糙度的变化。在该工艺参数下经过两次抛光后 RB-SiC 表面的粗糙度如图 8 所示。

从图 8 可以看到，飞秒激光抛光前 RB-SiC 基体的表面粗糙度约为 30 nm，在经过脉冲能量为 0.09 μJ

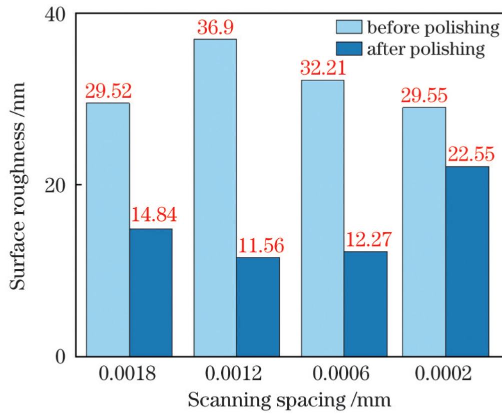

图 8 不同扫描间距下抛光前后的 RB-SiC 表面粗糙度

Fig. 8 Surface roughness of RB-SiC before and after polishing under different scanning spacing

的飞秒激光的抛光后，其表面粗糙度显著下降。在两次抛光后，随着扫描间距的减小，其表面粗糙度呈现出先减小后增加的趋势，当扫描间距为 0.0012 mm 时，得到的表面具有较低的粗糙度，为 11.56 nm，达到了较好的抛光效果，实现了 RB-SiC 表面的精密抛光。

此外，我们对不同扫描间距下抛光的表面形貌进行了分析，如图 9 所示。在飞秒激光抛光前，RB-SiC 基体表面经过 CeO_2 溶液抛光后，已相对平整，但仍然有大量凸起的毛刺。经过两次飞秒激光抛光后，RB-SiC 表面凸起的毛刺随着扫描间距的增加呈现先减少后增多的变化规律，与表面粗糙度的变化规律相同。当扫描间距为 0.0012 mm 时，其表面凸起的毛刺基本上已经被烧蚀去除，这也是其表面粗糙度最小的原因。此外，从图 9 还可以看出，当脉冲能量为 0.09 μJ 时，飞秒激光烧蚀去除的对象始终是 RB-SiC 基体表面凸起的毛刺，而毛刺的有效去除势必会导致其表面粗糙度降低。

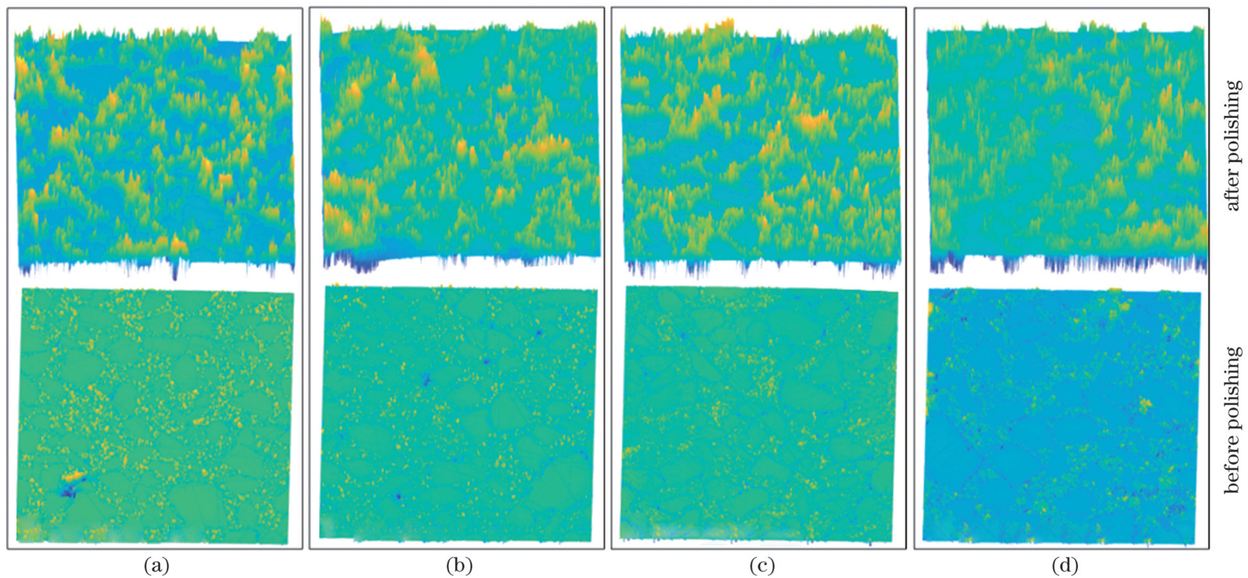

图 9 不同扫描间距下抛光前后的 RB-SiC 表面形貌。(a) 0.0018 mm；(b) 0.0012 mm；(c) 0.0006 mm；(d) 0.0002 mm

Fig. 9 Surface morphologies of RB-SiC before and after polishing under different scanning spacing. (a) 0.0018 mm; (b) 0.0012 mm; (c) 0.0006 mm; (d) 0.0002 mm

4 结 论

基于一维双温模型阐述了 RB-SiC 飞秒激光烧蚀过程，并通过区域烧蚀研究，分析了飞秒激光参数对表面粗糙度和烧蚀深度的影响规律。在此基础上，开展了 RB-SiC 表面的飞秒激光抛光工艺研究。结果表明：在飞秒激光与 RB-SiC 相互作用的过程中，飞秒激光脉冲使电子温度急剧上升，通过电子-声子耦合将热传递到晶格，晶格温度持续上升，而电子温度则逐渐下降，最终达到与晶格温度相同的温度，实现温度平衡。当脉冲能量密度达到其烧蚀阈值时，实现材料的去除。此外，飞秒激光区域烧蚀研究表明，通过飞秒激光抛光难以在 RB-SiC 切割表面上直接获得较高质量的表面，并且随着激光能量和光斑搭接率的增大，烧蚀表面粗糙度增大，烧蚀深度增大，但较小的扫描间距有利于获得平坦的烧蚀表面，有利于降低表面粗糙度。而在预抛光的 RB-SiC 表面上，通过飞秒激光烧蚀量的调控，可将其表面粗糙度从 36.9 nm 降至 11.56 nm，验证了飞秒激光抛光 RB-SiC 表面的可行性。后续可通过工艺参数的优化实现抛光效率的提升。

参 考 文 献

[1] East M, Knight J S, Allen L, et al. Material selection for far infrared telescope mirrors[J]. Proceedings of SPIE, 2018, 10698: 106891N.

[2] Kumar S. A review on Zerodur material strength behaviour with lightweighted design[J]. Materialstoday: Proceedings, 2021, 37(2):

3643-3645.

[3] Hull T B, Krieg J, Westerhoff T, et al. Parameters for mirror selection: trades between glass ceramics, glass, metals, ceramics and cordierites[J]. Proceedings of SPIE, 2020, 11443: 1144365.

[4] Da Deppo V, Pace E, Morgante G, et al. A prototype for the primary mirror of the ESA ARIEL mission: design and development of an off-axis 1-m diameter aluminum mirror for infrared space applications[J]. Proceedings of SPIE, 2018, 10706: 1070632.

[5] Da Deppo V, Pace E, Morgante G, et al. Study and realization of a prototype of the primary off-axis 1-m diameter aluminium mirror for the ESA ARIEL mission[J]. Proceedings of SPIE, 2019, 11180: 111806V.

[6] Greger R, Rugi E, Hausner T, et al. Development of technology for lightweight Beryllium Cassegrain Telescope for space applications and lessons learnt[J]. Proceedings of SPIE, 2017, 10564: 105643S.

[7] Mutters D K. Mirror topology optimization[J]. Proceedings of SPIE, 2019, 11100: 1110009.

[8] Dong Z C, Cheng H B. Ductile mode grinding of reaction-bonded silicon carbide mirrors[J]. Applied Optics, 2017, 56(26): 7404-7412.

[9] Nguyen T, Liu D, Thongkaew K, et al. The wear mechanisms of reaction bonded silicon carbide under abrasive polishing and slurry jet impact conditions[J]. Wear, 2018, 410/411: 156-164.

[10] Liang H Q, Yao X M, Zhang H, et al. Friction and wear behavior of pressureless liquid phase sintered SiC ceramic[J]. Materials & Design, 2015, 65: 370-376.

[11] Chen S S, Cheung C F, Zhang F H. An experimental and theoretical analysis of surface generation in the ultra-precision grinding of hard and brittle materials[J]. The International Journal of Advanced Manufacturing Technology, 2018, 97(5): 2715-2729.

[12] Zhang Q L, To S, Zhao Q L, et al. Impact of material microstructure and diamond grit wear on surface finish in micro-grinding of RB-SiC/Si and WC/Co carbides[J]. International Journal of Refractory Metals and Hard Materials, 2015, 51: 258-263.

[13] Wang X, Zhang X J. Theoretical study on removal rate and surface roughness in grinding a RB-SiC mirror with a fixed abrasive[J]. Applied Optics, 2009, 48(5): 904-910.

[14] 林晨, 许永超. 单晶蓝宝石衬底磨粒抛光技术研究现状[J]. 福建工程学院学报, 2021, 19(3): 216-222.
Lin C, Xu Y C. Research status of abrasive polishing technology for single crystal sapphire substrate[J]. Journal of Fujian University of Technology, 2021, 19(3): 216-222.

[15] Tam H Y, Cheng H B, Wang Y W. Removal rate and surface roughness in the lapping and polishing of RB-SiC optical components[J]. Journal of Materials Processing Technology, 2007, 192/193: 276-280.

[16] Zhou Y F, Zhang Y M, Han J C, et al. Design and fabrication of large-scale RB-SiC mirror[J]. Proceedings of SPIE, 2007, 6721: 67210S.

[17] Tang H D, Huang Z R, Tan S H. PVD SiC and PVD Si coatings on RB SiC for surface modification[J]. Proceedings of SPIE, 2006, 6149: 61490A.

[18] 康念辉, 李圣怡, 郑子文, 等. 典型碳化硅光学材料的超光滑抛光试验研究[J]. 中国机械工程, 2008, 19(21): 2528-2531, 2535.
Kang N H, Li S Y, Zheng Z W, et al. Experimental research on super-smooth polishing process of typical silicon carbide materials [J]. China Mechanical Engineering, 2008, 19(21): 2528-2531, 2535.

[19] Shen X M, Tu Q Z, Deng H, et al. Mechanism analysis on finishing of reaction-sintered silicon carbide by combination of water vapor plasma oxidation and ceria slurry polishing[J]. Optical Engineering, 2015, 54(5): 055106.

[20] Serrano P A A, Kim M, Kim D R, et al. Spherical mirror and surface patterning on silicon carbide (SiC) by material removal rate enhancement using CO_2 laser assisted polishing[J]. International Journal of Precision Engineering and Manufacturing, 2020, 21(5): 775-785.

[21] Yan Q S, Wang X, Xiong Q, et al. The influences of technological parameters on the ultraviolet photocatalytic reaction rate and photocatalysis-assisted polishing effect for SiC[J]. Journal of Crystal Growth, 2020, 531: 125379.

[22] Chen G M, Du C K, Ni Z F, et al. The effect of surface polarity on the CMP behavior of 6H-SiC substrates[J]. Russian Journal of Applied Chemistry, 2020, 93(6): 832-837.

[23] Yin X C, Li S J, Chai P. Investigation of SiC single crystal polishing by combination of anodic oxidation and mechanical polishing[J]. International Journal of Electrochemical Science, 2020, 15(5): 4388-4405.

[24] Park S H, Liu P P, Yi K, et al. Mechanical properties estimation of additively manufactured metal components using femtosecond laser ultrasonics and laser polishing[J]. International Journal of Machine Tools and Manufacture, 2021, 166: 103745.

[25] 任英明, 张志宇. 双步激光辐射提升纳秒激光抛光单晶硅的表面[J]. 光学学报, 2022, 42(7): 0714004.
Ren Y M, Zhang Z Y. Surface of nanosecond laser polished single-crystal silicon improved by two-step laser irradiation[J]. Acta Optica Sinica, 2022, 42(7): 0714004.

[26] 李欣欣, 李兴, 王翼猛, 等. 激光精密加工, 点亮智能制造[J]. 中国激光, 2022, 49(19): 1902001.
Li X X, Li X, Wang Y M, et al. Laser precision processing lightens intelligent manufacturing[J]. Chinese Journal of Lasers, 2022, 49(19): 1902001.

[27] Taylor L L, Qiao J, Qiao J E. Femtosecond laser polishing of optical materials[J]. Proceedings of SPIE, 2015, 9633: 96330M.

[28] 徐一帆, 邵景珍, 林颖, 等. 硬脆材料的激光表面抛光研究进展[J]. 激光与光电子学进展, 2022, 59(13): 1300003.
Xu Y F, Shao J Z, Lin Y, et al. Research progress of laser surface polishing of hard and brittle materials[J]. Laser & Optoelectronics Progress, 2022, 59(13): 1300003.

[29] Shao Y, Sun S F, Liu G L, et al. Laser-assisted thermochemical ultrahigh-precision polishing of titanium in phosphoric acid solution [J]. The International Journal of Advanced Manufacturing Technology, 2021, 115(4): 1201-1210.

[30] Zhao Y, Wang S, Yu W H, et al. Simulation and experimental study of laser processing NdFeB microarray structure[J]. Micromachines, 2023, 14(4): 808.

[31] Zheng Q Z, Cui J L, Fan Z J, et al. Investigation on the underwater femtosecond laser polishing SiC ceramic[J]. Ferroelectrics, 2020, 564(1): 28-36.

[32] Zheng Q Z, Cui J L, Fan Z J, et al. An experimental investigation of scan trajectory into the underwater femtosecond laser polishing SiC ceramic[J]. Ferroelectrics, 2020, 563(1): 77-86.

[33] Jiang L, Wang A D, Li B, et al. Electrons dynamics control by shaping femtosecond laser pulses in micro/nanofabrication: modeling, method, measurement and application[J]. Light: Science & Applications, 2018, 7(2): 17134.

[34] 刘聚坤, 赵宏伟, 王欢, 等. 利用双温模型理论分析飞秒激光烧蚀金过程[J]. 应用技术学报, 2018, 18(1): 63-66.
Liu J K, Zhao H W, Wang H, et al. Numerical simulation of femtosecond laser ablation Au by two-temperature model[J]. Journal of Technology, 2018, 18(1): 63-66.

[35] Hu W Q, Shin Y C, King G. Modeling of multi-burst mode pico-second laser ablation for improved material removal rate[J]. Applied Physics A, 2010, 98(2): 407-415.

[36] Zhang H Z, Wang H Y, Liu F F, et al. Investigation on femtosecond laser ablative processing of SiCp/AA2024 composites [J]. Journal of Manufacturing Processes, 2020, 49: 227-233.

[37] Kawamura T, Hori D, Kangawa Y, et al. Thermal conductivity of SiC calculated by molecular dynamics[J]. Japanese Journal of Applied Physics, 2008, 47(12): 8898-8901.

[38] van Driel H M. Kinetics of high-density plasmas generated in Si by 1.06-μm and 0.53-μm picosecond laser pulses[J]. Physical Review B, 1987, 35(15): 8166-8176.

[39] Choi T Y, Grigoropoulos C P. Plasma and ablation dynamics in ultrafast laser processing of crystalline silicon[J]. Journal of Applied Physics, 2002, 92(9): 4918-4925.

Study of Femtosecond Laser Ablation and Polishing Process on RB-SiC Surface

Chen Huan[1,2], Wei Chaoyang[1,2*], Cao Zhen[1,2**], Peng Xiaocong[1,2], Shao Jianda[1,2]

[1]*Precision Optical Manufacturing and Testing Center, Shanghai Institute of Optics and Fine Mechanics, Chinese Academy of Sciences, Shanghai* 201800, *China*;

[2]*Center of Material Science and Optoelectronics Engineering, University of Chinese Academy of Sciences, Beijing* 100049, *China*

Abstract

Objective Reaction-bonded silicon carbide (RB-SiC) is considered one of the most excellent and feasible materials for lightweight large telescope optics owing to its high specific stiffness and strength. It has broad application prospects in ultra-high-resolution astronomical observation, deep space exploration, and space situational awareness. However, the material has high hardness and a complex two-phase structure, which leads to a complex surface polishing and modification treatment process, low efficiency, and high cost. This has become a bottleneck limiting its further development. Although this problem can be solved using a femtosecond laser, which is a highly promising method for high-precision processing, few applications involving femtosecond lasers in RB-SiC have been reported, and the interaction processes and ablation patterns with RB-SiC remain unclear. Therefore, this study elucidates the interaction process between the femtosecond laser and the RB-SiC surface based on the one-dimensional two-temperature model. On this basis, research on the femtosecond laser ablation law and polishing process on the RB-SiC surface is conducted.

Methods RB-SiC is used in this study. First, the interaction process between the femtosecond laser and RB-SiC is clarified based on the two-temperature model. Second, the RB-SiC ablation law under the action of a femtosecond laser is studied experimentally, and the influence of various process parameters on the RB-SiC ablation during femtosecond laser scanning is analyzed. The process parameters for femtosecond laser polishing of the RB-SiC surface are preliminarily explored, providing a theoretical and experimental basis for its application as a polishing tool for RB-SiC surfaces.

Results and Discussions The process of RB-SiC femtosecond laser ablation is elaborated based on the dual-temperature model (Fig. 2), and the results show that during the interaction of the femtosecond laser with RB-SiC, the femtosecond laser pulse causes the electron temperature to rise sharply and transfers heat to the lattice through electron-phonon coupling, resulting in a continuous increase in lattice temperature, while the electron temperature gradually decreases. Finally, the electron and lattice reach the same temperature, resulting in material removal when the pulse energy density reaches the ablation threshold.

In addition, using experiments, the influence law of the ablation process parameters on the ablation effect is analyzed (Figs. 5–7), and the results show that process parameters such as pulse energy, pulse frequency, scanning speed, and scanning spacing have a significant influence on the ablation morphology. The increase in laser energy and pulse frequency and the decrease in scanning speed cause an increase in the ablation surface roughness and ablation depth. However, smaller scanning spacing benefits from the ablated surface flattening and surface roughness reduction. It is confirmed that it is difficult to obtain high surface quality on the RB-SiC cutting surface using femtosecond laser ablation.

On this basis, the femtosecond laser polishing process of the RB-SiC surface is explored (Figs. 8 and 9). The RB-SiC cutting surface is pre-polished with CeO_2 slurry for approximately 32 h, and this pre-polished surface is used as the basis for studying the femtosecond laser polishing process. The surface roughness of the RB-SiC substrate before femtosecond laser polishing is approximately 30 nm, which decreases significantly after femtosecond laser polishing with a pulse energy of 0.09 μJ. After polishing twice, the surface roughness shows a decreasing trend and subsequently increases with a decrease in the scanning spacing. At a scanning spacing of 0.0012 mm, a lower roughness surface can be obtained with a surface roughness of 11.56 nm, which achieves an improved polishing result. This indicates that the RB-SiC surface roughness after pre-polishing treatment can be effectively reduced by regulating the femtosecond laser ablation amount, and the feasibility of RB-SiC surface femtosecond polishing is initially verified.

Conclusions In this study, the femtosecond laser ablation process of RB-SiC is elaborated based on a one-dimensional two-temperature model, and the influence law of the femtosecond laser parameters on the surface roughness and ablation depth is analyzed using an area ablation study. Femtosecond laser polishing of the RB-SiC surface is subsequently performed. The results show that

during the interaction of the femtosecond laser with RB-SiC, the femtosecond laser pulse causes the electron temperature to rise sharply and transfers heat to the lattice through electron-phonon coupling, resulting in a continuous increase in the lattice temperature. The electron temperature gradually decreases and finally reaches the same temperature as the lattice achieves temperature equilibrium, which produces material removal when the pulse energy density reaches its ablation threshold. In addition, this study indicates that it is difficult to obtain a higher-quality surface directly using femtosecond laser polishing on the RB-SiC cutting surface. With an increase in laser energy and spot lap rate, the ablation surface roughness increases and the ablation depth increases, however, the smaller scan spacing facilitates the ablation surface flattening and assists in reducing surface roughness. However, on the pre-polished RB-SiC surface, the surface roughness can be polished from 36.90 nm to 11.56 nm by regulating the femtosecond laser ablation amount, which verifies the feasibility of polishing the RB-SiC surface using the femtosecond laser. Femtosecond laser polishing efficiency can be improved by the subsequent optimization of process parameters, and this is expected to address the challenge of low efficiency RB-SiC polishing.

Key words laser technique; roughness; reaction bonded silicon carbide (RB-SiC); femtosecond laser polishing; two-temperature model